Spectroscopic study of ^{38}K above the 31.67 μs isomer

Rozina Rahaman,[1] Abhijit Bisoi,[1,*] Y. Sapkota,[1] Anik Adhikari,[1] Ananya Das,[1] S. Sarkar,[1] M. Saha Sarkar,[2] A. Goswami,[2] S. Ray,[3] M. Roy Basu,[4] Debasmita Kanjilal,[5] Somnath Nag,[6] K. Selvakumar,[7] N. Madhavan,[8] S. Muralithar,[8] and R. K. Bhowmik[8]

[1]*Indian Institute of Engineering Science and Technology, Shibpur, Howrah-711103, India*
[2]*Saha Institute of Nuclear Physics, Bidhannagar, Kolkata-700064, India*
[3]*Department of Nuclear Science and Technology, Mody University of Science and Technology, Sikar, Rajasthan-332311, India*
[4]*Department of Physics, University of Calcutta, Kolkata-700009, India*
[5]*Department of Physics, Raiganj Surendranath Mahavidyalaya, Raiganj-733134, India*
[6]*Indian Institute of Technology (Banaras Hindu University), Varanasi-221005, India*
[7]*Department of Physics, Bannari Amman Institute of Technology, Sathyamangalam-638401, India*
[8]*Inter-University Accelerator Centre, New Delhi-110067, India*

(Received 15 April 2020; revised 22 June 2020; accepted 14 July 2020; published 13 August 2020)

High-spin states of ^{38}K above the 31.67 μs (τ_m) isomer, populated through the ^{12}C(^{28}Si, np)^{38}K reaction with a 110 MeV ^{28}Si beam, have been studied by using the Indian National Gamma Array (INGA) facility. Two new levels and four new transitions have been added to the existing level scheme. The spins and parities of most of the levels above the isomer have been assigned, modified, and confirmed from $R_{\rm DCO}$, $R_{\rm ADO}$, and linear polarization measurements. The multipole mixing ratios (δ) for a few transitions have been measured. Large-basis shell-model calculations have been performed to understand the microscopic origin of these levels. In our calculations, different particle restrictions in sd- and pf-shell orbitals were used to reproduce the experimental level energies. Two-nucleon transfer spectroscopic factors have also been calculated for the levels above the isomer to support the new spin and parity assignments. Prediction of collective excitation at high excitation energy in ^{38}K is also discussed.

DOI: 10.1103/PhysRevC.102.024315

I. INTRODUCTION

Nuclei in the neighborhood of doubly closed ^{40}Ca usually exhibit the characteristic of spherical single-particle excitation spectra [1] and their excitation spectra are well explained by the spherical shell model [2–7]. Recent developments of detector and data-acquisition systems made it possible to study these nuclei at higher angular momentum and excitation energy. As a result, the coexistence of single-particle and collective excitations have been observed in a few sd shell nuclei, viz., ^{40}Ca [8], ^{36}Ar [9], ^{35}Cl [10], etc. In these nuclei, the single-particle excitations are mostly dominant at low excitation energies and collective excitations in terms of normal deformed or even superdeformed (SD) bands are found at relatively higher excitation energies. Shell-model calculations with multiparticle multihole excitation have been performed successfully to understand the microscopic origin of these observed SD bands. The origin of the observed SD bands in ^{40}Ca [8], ^{36}Ar [9], ^{35}Cl [10] nuclei are explained in terms of 8p-8h [11], 4p-4h [12], and 3p-3h [10] excitations, respectively, in shell-model calculations. The presence of α-cluster structure of the states of these SD bands has already been discussed in Refs. [10,13,14]. The presence of α clusters at low excitation energy has been predicted recently in the non-α-conjugate ^{34}S nucleus [15]. The α-cluster structure in ^{34}S and ^{35}Cl has been studied by using shell-model calculations [10,15]. Therefore, this region gives us an opportunity to investigate experimentally the interplay between single-particle and collective-mode excitations and interpret them theoretically by using large-basis shell-model calculations.

^{38}K is an odd-odd ($N = Z = 19$) nucleus in the upper sd shell. In the recent past, we investigated the high-spin structure of a few upper sd shell nuclei, viz., ^{33}S [2], ^{34}Cl [3], ^{35}Cl [10], and ^{37}Ar [7]. The low-lying states of these nuclei are primarily generated from single-particle excitations. However, at higher excitation energy, the signature of collective excitation has been found. In ^{35}Cl, a superdeformed band has been observed above 8 MeV excitation energy. A candidate superdeformed band has been identified in ^{33}S [2] above 3 MeV excitation energy. In ^{34}Cl and ^{37}Ar, large configuration mixing in terms of different particle partitions in their calculated wave functions obtained from shell-model calculations clearly indicate the presence of collective excitations at higher excitation energy. It has also been noted that two normal deformed bands generated from 4p-4h excitation have also been reported in ^{38}Ar [16]. ^{38}Ar is the isobaric partner nucleus of ^{38}K. So, one may also expect collective excitations at higher excitation energy in ^{38}K, generated from multiparticle multihole excitations.

*abhijitbisoi@physics.iiests.ac.in

^{38}K has been substantially investigated through proton-, deuteron-, and alpha-induced reactions [1]. However, only a few experimental data are available where heavy-ion beams were used [1]. Mostly the low-lying level structure of ^{38}K has been investigated through these experiments. Several attempts have also been made to measure the mean life ($\tau_m = 31.67\ \mu$s) of 3.458 MeV $(7)^+$ isomeric level. But the high-spin level structure of ^{38}K above this isomer is not well studied. The ^{38}K nucleus was previously studied by C. J. van der Poel *et al.* [17] through heavy-ion reactions. They extended the level scheme up to 11 MeV and assigned the spin and parity of a few levels by the directional correlation of γ rays emitted from excited states (DCO) measurements or shell-model calculation. We have found that the spin and parity of a few levels below the isomer were only confirmed and for all the levels above the isomer, these were not confirmed. Our primary motivation is, therefore, to investigate the high-spin structure of ^{38}K and search for collective excitations at high excitation energy in ^{38}K. Our preliminary work on ^{38}K was already reported in Ref. [18].

In the present work, we primarily study the level scheme of ^{38}K above the 3.458 MeV isomer. We have added four new transitions and two new levels to the existing level scheme. The directional correlation of γ rays emitted from excited states (DCO), the angular distribution from oriented nuclei (ADO), and the integrated polarization directional correlation of oriented nuclei (IPDCO) measurements have been carried out to assign the spin and parity of the level. The large-basis shell-model (LBSM) calculations with different particle restrictions in the model space have been carried out to understand the microscopic origin of these states. It has been reported in Ref. [17] that the spin and parity of the levels above the isomer were assigned tentatively (within double brackets) based on their correlation with the low-lying level structure of ^{36}Ar. In the present work, we therefore calculate two-nucleon transfer spectroscopic factors by using a shell-model calculation to understand the correlation between the two nuclei ^{36}Ar and ^{38}K. The presence of collective excitations in terms of configuration mixings in ^{38}K is also discussed. Based on our calculations, we also predict the possibility to have a deformed band in ^{38}K.

II. EXPERIMENTAL DETAILS

High-spin states in ^{38}K were populated through the ^{12}C(^{28}Si, np)^{38}K reaction in the inverse kinematics with a 110 MeV ^{28}Si beam. The ^{28}Si beam was provided by the 15UD Pelletron accelerator at the Inter-University Accelerator Centre (IUAC), New Delhi. The target was ^{12}C (50 μg/cm^2) evaporated on 18 mg/cm^2 Au backing. A multidetector array (Indian National Gamma Array, setup) comprising 13 Compton-suppressed clovers were used to detect the γ rays. These thirteen clovers were mounted at five different angles, i.e., 148°(4), 123°(2), 90°(4), 57°(2), and 32°(1) with respect to the beam axis. The relevant details of the experimental setup have been discussed in Ref. [19]. The time width of the coincidence condition was 200 ns. About 10^8 twofold coincidence events were recorded in list mode. The experimental data have been sorted into angle-independent symmetric and angle-dependent asymmetric γ-γ matrices to extract the spectroscopic information of the detected gammas. The data have been analyzed by using the analyzing program INGASORT [20].

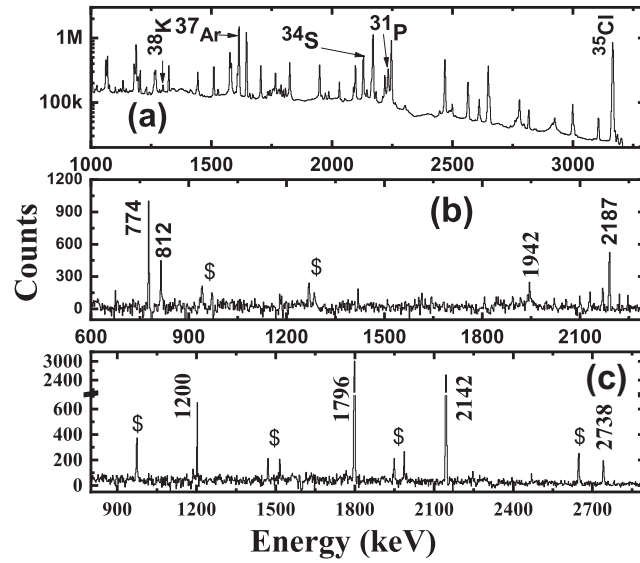

FIG. 1. (a) A total projection spectrum of γ rays emitted by different nuclei from the present experiment. Background-subtracted coincidence spectra obtained by putting a gate on (b) 328 keV (below the isomer) and (c) 1296 keV (above the isomer) transitions. Transitions marked with $ are from contaminants.

The energy calibration of the clovers were performed with ^{152}Eu and ^{133}Ba radioactive sources. These sources emitted γ rays having energies up to 1408 keV only and we could not consider the high-energy room background gammas (like 2614 keV) during energy calibration due to their low statistics. So, we used a few online gammas energy ranges from 600 to 3200 keV to estimate the energy calibration uncertainties in the high-energy region. The relative efficiency calibrations of the clovers were performed with ^{152}Eu, ^{133}Ba, and ^{66}Ga radioactive sources. The ^{66}Ga source having gamma energy 833 to 4806 keV was prepared through ^{52}Cr(^{16}O, pn)^{66}Ga reaction at 55 MeV [21]. The uncertainty in the efficiency has been estimated from the efficiency curve fitting. We used the sorting program INGASORT [20] for this fitting.

III. RESULTS AND DISCUSSION

The level scheme of ^{38}K has been studied based on the coincidence relationship, relative intensities, $R_{\rm DCO}$, $R_{\rm ADO}$, and IPDCO ratios of γ rays. A total projection spectrum, as well as typical gated spectra, are shown in Fig. 1. The PACE4 [22] predicted relative cross section of the ^{12}C(^{28}Si, np)^{38}K channel is 8.3% of the total fusion. The γ rays from nuclei populated through other dominant channels of the reaction are therefore marked in Fig. 1(a). Since there is an isomer of mean life (τ_m) = 31.67(16) μs [17] at 3.458 MeV, the level scheme of ^{38}K is studied by putting gates both above and below the isomer. Below the 3.458 MeV isomer, we could not find any new transitions. The 1942 keV transition was found in the 328 keV gated spectrum, which was already observed in light-

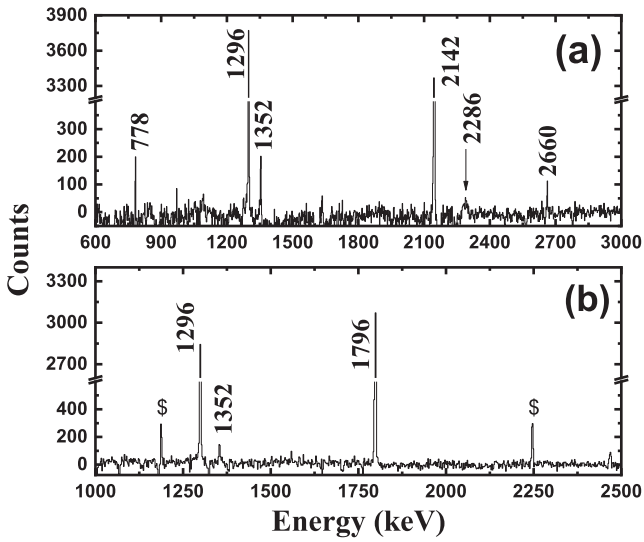

FIG. 2. Background-subtracted coincidence spectra obtained by putting a gate on (a) 1796 keV and (b) 2142 keV transitions. Transitions marked with $ are from contaminants.

ion-induced experiments [1]. We have identified four new transitions (viz., 778, 1200, 2660, and 2738 keV) above the 3.458 MeV isomer. It has been found that, among these four transitions, 778 and 2660 keV transitions are in coincidence with each other and also in coincidence with the 1796 keV transition. But these transitions are not in coincidence with the 1296 and 2142 keV transitions [Figs. 1(c) and 2(b)]. Similarly, 1200 and 2738 keV transitions are in coincidence with each other and also with the 1296 keV transition. But these transitions are not in coincidence with the 1796 and 2142 keV transitions [Figs. 2(a) and 2(b)]. To place them in the level scheme, we need to know their relative intensities. In the present work, we have only measured the relative intensities of 778 and 2660 keV transitions from the 1796 keV gated spectrum. The relative intensity of the 2660 keV transition is more than that of the 778 keV transition (Table I). We therefore placed 778 keV above the 2660 keV transition. Since the 1200 and 2738 keV transitions are not in coincidence with the 1796 keV transition, we could not measure their relative intensities from the 1796 keV gated spectrum. It is also not possible to find out the relative intensities of these transitions from the 812 keV gated spectrum due to the presence of the 31.67(16) μs isomer [17] at 3.458 MeV. So, we measured the intensities of these transitions from the 1296 keV gated spectrum. The measured intensities of the 1200 and 2738 keV transitions are 1926(143) and 2257(181), respectively. Since the intensity of the 2738 keV transition is more than that of the 1200 keV transition, we placed the 1200 keV transition above the 2738 keV transition. Therefore, two new levels (6196 and 7914 keV) have been added above the 31.67(16) μs isomer. For the relative intensity measurement, we generally put a gate on a transition which is below the transition of interest (bottom gate). In this case, we put the gate on the 1296 keV transition, which is above the transitions (1200 and 2738 keV) of interest (top gate). The position of the new 6196 keV level is therefore assigned as tentative and represented by the dotted line in the level scheme (Fig. 3).

The placement of the existing levels, viz., 5254, 7396, 8692, 8748, and 10 978 keV [17] has been confirmed from the coincidence relationship and relative intensities of the decay out 1796, 2142, 1296, 1352, and 2286 keV transitions. Figures 1(c) and 2 clearly show the coincidence relationship between the 1796, 2142, 1296, and 1352 keV transitions. Due to the weak statistics and large Doppler boarding, the 2286 keV transition is not clearly visible in 1296 and 2142 keV gated spectra. These spectra were generated from an all angle vs all angle symmetric matrix. We therefore generated 1796, 2142, and 1296 keV gated spectra from a 90° vs 90° symmetric matrix to check their coincidence relation with the 2286 keV transition. It shows from Figs. 4(a)–4(c) that they are in coincidence with the 2286 keV transition. The 2286 keV gated spectrum is shown in Fig. 4(d), where the 1296, 1796,

TABLE I. Relative intensity I_{rel}, R_{DCO}, R_{ADO}, Δ_{IPDCO}, and mixing ratio (δ) of the γ transitions in ^{38}K. I_{rel} has been measured from 1796 keV gated spectrum. Since the spin and parity of the 3458 keV level has been established as 7^+ from the results obtained from shell-model calculations, we quote the spin and parity of the levels above the isomer, which have been confirmed in the present work, without brackets.

E_γ	E_X				E_{gate}				Δ_{IPDCO}		
keV	keV	I_{rel}	J_i^π	J_f^π	keV	ΔJ	R_{DCO}	R_{ADO}	Expt.	Theor.	Mixing ratio (δ)
778(1)	8692	1.9(2)	11^-	$9_2^{(+)}$	1796	1	1.8(5)	1.1(2)			+0.1(3)
1200(1)	7396		9^-	$9_1^{(+)}$	1296	2	1.6(5)	1.7(3)			
1296(1)	8692	47(3)	11^-	9^-	1796	1	1.7(3)	1.5(2)	+0.11(5)	+0.05	$E2$
					2142	1	1.8(3)	1.5(2)			
1352(1)	8748	3.8(3)	$10^{(+)}$	9^-	2142	1		0.8(2)			
1796(1)	5254	100(5)	8^+	7^+	1296	2	0.57(8)	0.71(8)	−0.02(4)	−0.02	+0.05(5)
					2142	1	1.02(14)	0.8(1)			
2142(1)	7396	77(4)	9^-	8^+	1296	2	0.50(8)	0.70(8)	+0.07(4)	+0.02	+0.01(2)
					1796	1	1.03(15)	0.80(9)			
2286(2)	10 978	6.6(6)	$12^{(-)}$	11^-	1796	1		0.54(10)			
2660(2)	7914	2.4(3)	$9_2^{(+)}$	8^+	1796	1		0.6(2)			
2738(2)	6196		$9_1^{(+)}$	7^+	1296	2	1.2(3)	1.3(3)			

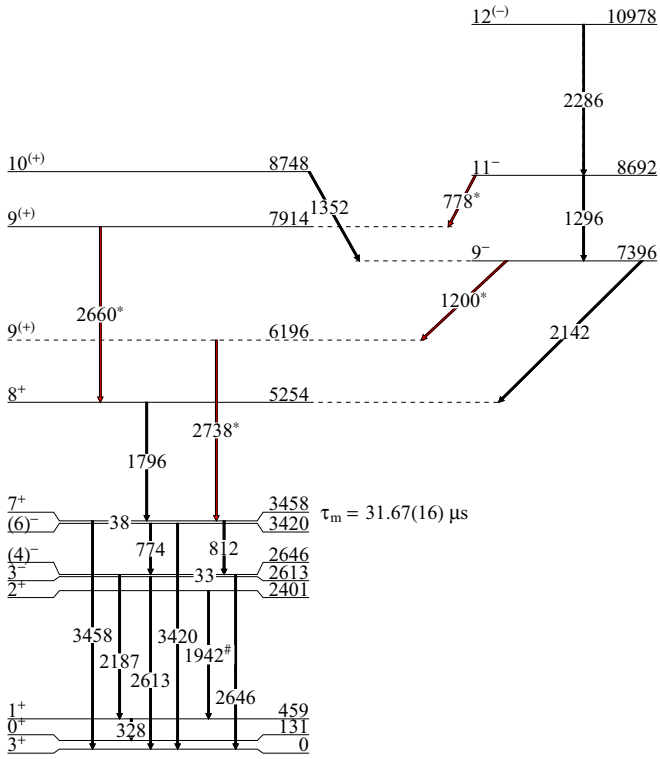

FIG. 3. Partial level scheme of ^{38}K. Energy levels are given in keV. Newly assigned γ transitions and those already observed in light-ion-induced reactions are indicated by $*$ and #, respectively. The spins and parities of the levels below the isomer are taken from Refs. [1,17]. Since the spin and parity of the 3458 keV level has been established as 7^+ from the results obtained from shell-model calculations, we quote the spin and parity of the levels above the isomer which are confirmed in the present work, without brackets.

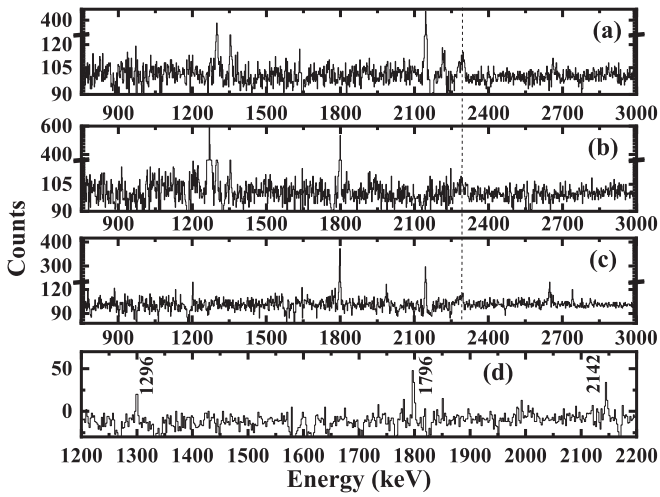

FIG. 4. Background-subtracted coincidence spectra obtained by putting a gate on (a) 1796 keV (b) 2142 keV, and (c) 1296 keV transitions. The position of the 2286 keV transition in panels (a)–(c) is marked by a dotted line. The background-subtracted coincidence spectrum obtained by putting a gate on the 2286 keV transition is shown in panel (d). These spectra were generated from a 90° vs 90° symmetric matrix.

and 2142 keV transitions are present. The 1352 keV transition is, however, not observed in Fig. 4(d). These observations confirm that the 2286 keV transition is in coincidence with the 1296, 1796, and 2142 keV transitions but not in coincidence with the 1352 keV transition. The position of the 10 978 keV level [17] is therefore confirmed in the present work. The relative intensities of the 1296, 1352, 2142, and 2286 keV transitions were measured from the 1796 keV gated spectrum. The relative intensity of the 1796 keV transition was measured from the total projection spectrum with proper normalization. The results are shown in Table I.

To confirm or assign the spins and parities of the levels in ^{38}K, the measurement of the directional correlation of γ rays emitted from excited states (DCO) was carried out. The DCO ratio ($R_{\rm DCO}$) [23] of a γ transition (γ_1) is defined as the ratio of intensities of that γ ray ($I\gamma_1$) for two different angles in coincidence with another γ ray (γ_2) of known multipolarity. The DCO ($R_{\rm DCO}$) is expressed as

$$R_{\rm DCO} = \frac{I^{\gamma_1} \text{ observed at angle } \theta, \text{ gated by } \gamma_2 \text{ at } 90^\circ}{I^{\gamma_1} \text{ observed at angle } 90^\circ, \text{ gated by } \gamma_2 \text{ at } \theta}. \quad (1)$$

The $R_{\rm DCO}$ value depends on the multipolarities of these transitions (γ_1 and γ_2), and the angle between the detectors. For the stretched transitions of the same multipolarities, the DCO value is close to unity and for a stretched dipole (quadrupole) transition gated by a pure quadrupole (dipole) transition, it is nearly 0.5(2). For a mixed transition, it deviates from unity or 0.5(2).

The experimental data have been sorted into different angle-dependent asymmetric matrices for DCO measurement. In this analysis, the DCO ratios have been determined for $\theta = 148^\circ$. The DCO measurement has been carried out mostly by putting a gate on such a transition whose multipolarity and mixing ratio is known. In ^{38}K, the multipolarities of a few low-lying transitions were only confirmed. But we could not use them in DCO measurement due to the presence of the 31.67 μs isomer at 3.458 MeV. Therefore, we only performed the DCO measurements for a few transitions above the isomer. Since the spin and parity of all the levels above the isomer are not confirmed, we put the gate on a transition whose multipolarity is still not confirmed.

In the present work, the DCO measurements have been carried out for the 778, 1200, 1296, 1796, 2142, and 2738 keV transitions (Table I). The $R_{\rm DCO}$ values of the 778, 1296, and 2142 keV transitions obtained from the 1796 keV gated spectrum are 1.8(5), 1.7(3), and 1.03(15), respectively. For the 1200, 1796, 2142, and 2738 keV transitions, $R_{\rm DCO}$ values obtained from the 1296 keV gated spectrum are 1.6(5), 0.57(8), 0.50(8), and 1.2(3), respectively. Similarly, the $R_{\rm DCO}$ values of the 1296 and 1796 keV transitions obtained from the 2142 keV gated spectrum are 1.8(3) and 1.02(14), respectively. Large uncertainties in the measured DCO values of 778, 1200, and 2738 keV transitions are due to their low statistics and poor peak shape in the gated spectra. The results therefore confirm that the 1796 and 2142 keV transitions have the same multipolarities. Similarly, the multipolarities of the 778, 1296, and 2738 keV transitions are same but differ from those of the 1796 and 2142 keV transitions. To assign the dipole and quadrupole nature of these transitions, we measured the $R_{\rm DCO}$

TABLE II. R_{DCO} and R_{ADO} values of the known γ transitions in ^{35}Cl.

E_γ keV	J_i^π	J_f^π	E_{gate} keV	ΔJ	R_{DCO}	R_{ADO}
518	$7/2^-$	$7/2^+$	680	1	1.5(2)	1.6(4)
972	$17/2^+$	$13/2^+$	680	1	1.8(2)	1.6(2)
			2646	2	0.9(1)	
1702	$9/2^-$	$7/2^+$	2646	2	0.49(6)	0.60(6)
1946	$13/2^+$	$11/2_2^-$	2646	2	0.45(8)	0.59(8)
2466	$13/2^+$	$11/2_1^-$	2646	2	0.51(8)	0.65(9)
2646	$7/2^+$	$3/2^+$	680	1	1.7(2)	1.6(2)

of a few known transitions in ^{35}Cl populated in the same experiment. It has been found that the R_{DCO} of a quadrupole (dipole) transition gated by dipole (quadrupole) transition is close to 2.0(0.5), as shown in Table II. Therefore, based on the measured R_{DCO} values of the 778, 1296, 1796, 2142, and 2738 keV transitions, we conclude that the 778, 1296, and 2738 keV transitions are quadrupole transitions and both the 1796 and 2142 keV transitions are dipole transitions.

In the case of the 1200 keV transition, the measured R_{DCO} value, obtained from the quadrupole gated spectrum, is 1.6(5). Since the measured R_{DCO} value of a dipole transition gated by a quadrupole transition is close to 0.5, as shown in Tables I and II, and both the $\Delta J = 0$ and $\Delta J = 2$ transitions show similar R_{DCO}, we have assigned 1200 keV as the $\Delta J = 0$ transition.

The DCO measurement could not be carried out for other transitions, viz., 1352, 2286, and 2660 keV due to their low statistics. So, the angular distribution from oriented nuclei (ADO) measurements have been carried out to determine their multipolarities. Two asymmetric matrices have been constructed for the ADO measurement. In the first matrix, the events from all angle (except 90°) detectors are stored in the first axis and in the second axis we store the events from the 90° detectors only. Similarly, in the second matrix, the events from all angle (except 148°) detectors are stored in the first axis and in the second axis we store the events from the 148° detectors only. The ADO (R_{ADO}) [24] of a transition is then defined as

$$R_{ADO} = \frac{I_{\gamma_1} \text{ measured at } \theta = 148^\circ;\ \text{gated by } \gamma_2 \text{ at all}}{I_{\gamma_1} \text{ measured at } \theta = 90^\circ;\ \text{gated by } \gamma_2 \text{ at all}}. \quad (2)$$

For the present setup, R_{ADO} is 0.6 for the pure dipole transition and 1.6 for the pure quadrupole transition and the $\Delta J = 0$ transition (Table II). In the case of mixed transitions, depending on the extent of mixing (δ), R_{ADO} may change from these values. The ADO measurements have also been carried out for 778, 1200, 1296, 1796, 2142, and 2738 keV transitions whose multipolarities have already been evaluated from the DCO measurements. The results obtained from ADO measurements are tabulated in Table I. The R_{ADO} values of the 1200, 1296, 1796, 2142, and 2738 keV transitions are consistent with their assigned multipolarities. In case of the 778 keV transition only, the measured R_{ADO} value [1.1(2)] is largely deviated from the expected R_{ADO} value (1.6) of a pure quadrupole transition (Table II). This is may be due to

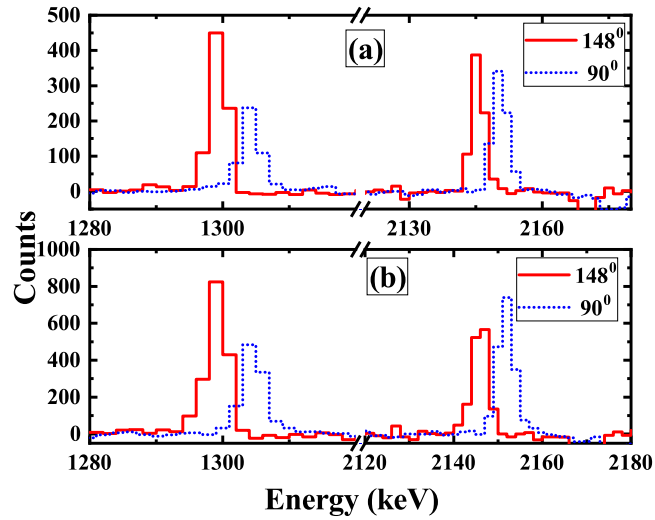

FIG. 5. A schematic representation of (a) DCO and (b) ADO spectra in ^{38}K. These two spectra (a) and (b) are generated by putting gates on the 1796 keV transition. The 90° spectra have been artificially shifted by 5 keV for a clear view.

the presence of large mixing (δ) in the 778 keV transition. The measured R_{ADO} values of the 1352, 2286, and 2660 keV transitions are 0.8(2), 0.54(10), and 0.6(2), respectively, which confirm their dipole nature. A schematic representation of DCO and ADO spectra are shown in Fig. 5.

The integrated polarization directional correlation of oriented nuclei (IPDCO) [25] measurement has been performed to assign the electric or magnetic nature of the transition. Two asymmetric matrices named parallel and perpendicular matrices were therefore constructed for the IPDCO measurement. In the parallel (perpendicular) matrix, the simultaneous events detected in the two crystals of 90° clovers which are parallel (perpendicular) to the emission plane are recorded on the first axis and on the second axis, the coincident γ rays detected in any other clover detector are recorded. The polarization asymmetry is then expressed as

$$\Delta_{IPDCO} = \frac{a(E_\gamma)N_\perp - N_\parallel}{a(E_\gamma)N_\perp + N_\parallel}, \quad (3)$$

where $N_\perp$ and $N_\parallel$ are the intensities of full peak observed in the perpendicular and parallel matrices, respectively. The asymmetry correction factor $a(E_\gamma)$ represents the geometrical asymmetry of the clovers placed at 90°. It is defined as

$$a(E_\gamma) = \frac{N_\parallel}{N_\perp}. \quad (4)$$

In the present work, ^{152}Eu radioactive source was used to extract the asymmetry correction factor $a(E_\gamma)$. To measure the Δ_{IPDCO} of the transition, we put a gate on coincident γs on the second axis and measured the intensities of the transition of interest from the projected parallel and perpendicular spectra. The positive value of Δ_{IPDCO} implies a pure electric transition whereas the negative value indicates a pure magnetic transition. For a mixed transition, the value comes close to zero and the sign depends on the amount of mixing. In our detector

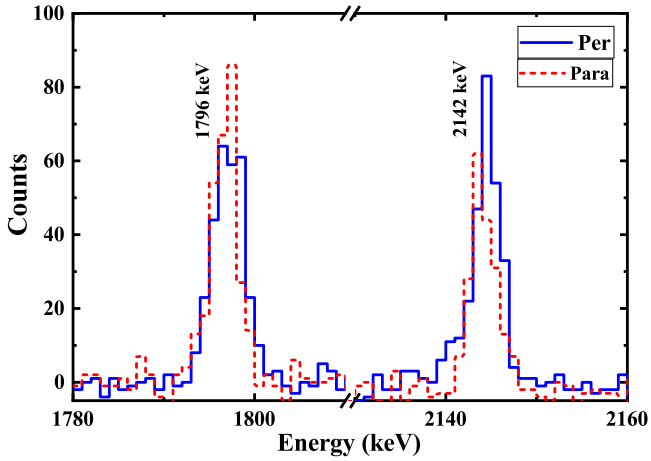

FIG. 6. Spectra generated from perpendicular and parallel matrices indicating the electric (magnetic) nature of the 2142 keV (1796 keV) transition.

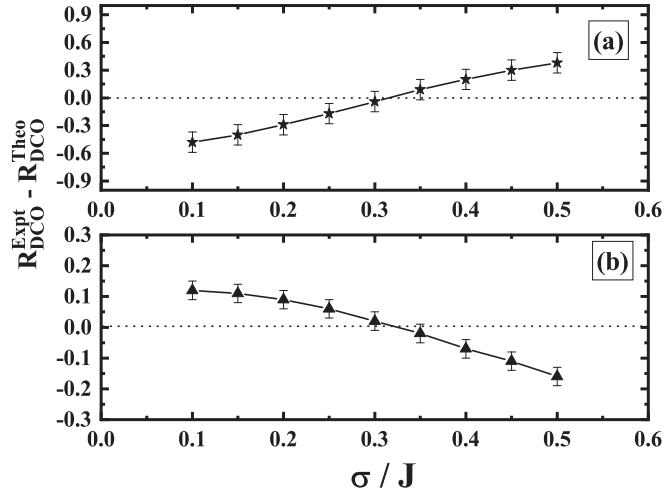

FIG. 7. Difference between the experimental R_{DCO} and theoretical R_{DCO} values of (a) 972 [$E2$: $\delta = 0$] keV and (b) 1702 [$E1$: $\delta = -0.002(1)$] keV transitions of ^{35}Cl as a function of σ/J.

setup, four clovers were mounted at 90°, but only two of them were suitable for polarization measurement. So, the IPDCO measurements have been carried out with two clovers placed at 90°. As a result, we only measured the Δ_{IPDCO} for three strong transitions, viz., 1296, 1796, and 2142 keV in ^{38}K. The results are shown in Table I. It confirms the electric nature of the 1296 and 2142 keV transitions and the magnetic nature of the 1796 transition. Figure 6 shows the spectra obtained from parallel and perpendicular matrices. Comparison of these projected spectra clearly shows the magnetic and electric nature of the 1796 and 2142 keV transitions.

To assign or confirm the spin and parity of the levels above the 3.458 MeV isomer, one should first confirm the spin and parity of the 3.458 MeV isomeric level. The spin and parity of the 3.458 MeV level was previously assigned as $(7)^+$ [17]. In the present work, we are not able to confirm experimentally the spin and parity of this level. However, the calculated energy and the lifetime of the 7^+ level obtained from shell-model calculations matches excellently with the reported excitation energy and lifetime of the $(7)^+$ [17] level. The details of the calculations are discussed in the next section. Therefore, we have established the spin and parity of the 3.458 MeV level as 7^+. Based on the R_{DCO}, R_{ADO}, and Δ_{IPDCO} values of the 1296, 1796, and 2142 keV transitions, we therefore assign the spin and parity of the 5254, 7396, and 8692 keV levels as 8^+, 9^-, and 11^-, respectively (Fig. 3). Previously, these levels were assigned as $((9^+))$, $((10^-))$, and $((12^-))$, respectively [17]. In the present work, only the DCO or/and ADO measurements were carried out for the four new transitions, viz., 778, 1200, 2660, and 2738 keV, but the polarization measurements were not performed due to their low statistics. So, we have only confirmed the spins of the two new 6196 and 7914 keV levels as $9_1^{(+)}$ and $9_2^{(+)}$, respectively (Fig. 3). We assign the parities of these levels by using the results obtained from shell-model calculations (discussed in the next section). Similarly, the spins and parities of 8748 and 10 978 keV levels have been assigned as $10^{(+)}$ and $12^{(-)}$, respectively, based on the R_{ADO} values of the decay out transitions and the results obtained from shell-model calculations (Fig. 3). Previously, these levels were assigned as $((11^-))$ and $((13^-))$, respectively [17].

For extracting the γ-ray multipole mixing ratios (δ), we compare the experimental DCO values with the theoretical values calculated by using the computer code ANGCOR [23]. The spin alignment parameter $\sigma/J = 0.3$, obtained from a few known $E1$ and $E2$ transitions (Fig. 7), was used for this calculation. The mixing ratios (δ) of the 778, 1796, and 2142 keV transitions obtained from the present work are 0.1(3), 0.05(5), and 0.01(2), respectively. The mixing ratios (δ) of the 1796 and 2142 keV transitions are then used to calculate the theoretical Δ_{IPDCO} of the 1796 and 2142 keV transitions. The results are shown in Table I.

In the next section we compare our experimental observation with the shell-model results and discuss in detail these new assignments. In the present work, uncertainties quoted in the measured values of intensities, R_{DCO} and R_{ADO}, are due to the statistical errors and the errors from the detector efficiency. The uncertainties quoted in the gamma energy are extracted from peak fitting and detector calibration errors. Since we have not considered efficiency corrections for polarization measurements, the uncertainties quoted in the Δ_{IPDCO} measurements are statistical only.

IV. THEORETICAL CALCULATION

Large-basis shell-model calculations were performed by using the code OXBASH [26] to understand the microscopic origin of each state in ^{38}K. The valence space consists of both *sd-pf* major shells with $1d_{5/2}$, $1d_{3/2}$, $2s_{1/2}$, $1f_{7/2}$, $1f_{5/2}$, $2p_{3/2}$, and $2p_{1/2}$ orbitals for both protons and neutrons above the ^{16}O inert core. ^{38}K is a self-conjugate nucleus and the number of valence particles (protons + neutrons) in ^{38}K is 22. The *SDPFMW* interaction [27] (as referred to within the OXBASH [26] code package) was used for the calculation. Other relevant details of the interaction and calculation are discussed in Ref. [5].

Unrestricted calculations for a nucleus having such a large number of valence particles in the full *sd*-*pf* space are often not possible due to the large *m*-scheme basis dimension. Therefore, several particle restrictions in the model space are used for shell-model studies of these nuclei. The results for energy spectra and transition probabilities in ^{38}K with different particle restrictions are discussed in the next sections. For all of these calculations, the mass normalization factor which is defined as the number of particles up to the *sd* shell is taken accordingly.

A. Positive-parity states

We have used two different truncation schemes named Theo-P1 and Theo-P2 to reproduce the positive-parity states in ^{38}K.

1. Theo-P1

In Theo-P1, only $0\hbar\omega$ excitation was considered, i.e., only the full *sd* shell was taken as the model space. The mass normalization factor for *sd*-shell two-body matrix elements (TBMEs) for this calculation was 38. The calculated ground-state binding energy of ^{38}K is -251.345 MeV, which agrees well with the experimental binding energy of -251.165 MeV (corrected for the Coulomb energy) [28]. The calculated excitation energies of 0^+, 1^+, and 2^+ also match well with the experimental energies. The maximum possible spin which can be generated in full *sd* model space for ^{38}K is 5^+. So, we have to consider the contribution from the neighboring *pf* orbitals to generate the high-spin positive-parity states (>5).

2. Theo-P2

In Theo-P2, we include all the *pf* orbitals in our calculations and allow excitation of only two particles into the *pf* shell to generate the high-spin positive-parity states. The mass normalization factor for this calculation was taken to be 36. We discussed earlier that the spins and parities of all the levels above the 3458 keV isomer were not confirmed due to the ambiguity of the spin and parity of the isomeric level. To remove this ambiguity, we compare the energies of the experimental levels with the shell-model results (Fig. 8). It shows that the experimental energy of the $(7)^+$ level [17] is very close to the calculated energy of the 7^+ level generated from pure 2p-2h excitation. The calculated lifetime of the 7^+ level (31.4 μs) (using the result of Theor$_2$ from Table III) also agrees well with the measured lifetime of the $(7)^+$ state (31.7 μs). Based on these observations, we have therefore established the spin and parity of the 3458 keV level as 7^+. The calculated energy of the 8^+ level agrees well with the experimental energy of the newly assigned 8^+ level. It has also been found that the experimental energies of $J = 9_1$, 9_2, and 10 levels ($E_x = 6196$, 7914, and 8748 keV, respectively) are close to the calculated energies of 9_1^+ (6625 keV), 9_2^+ (8112 keV), and 10^+ (8877 keV), respectively. However, the

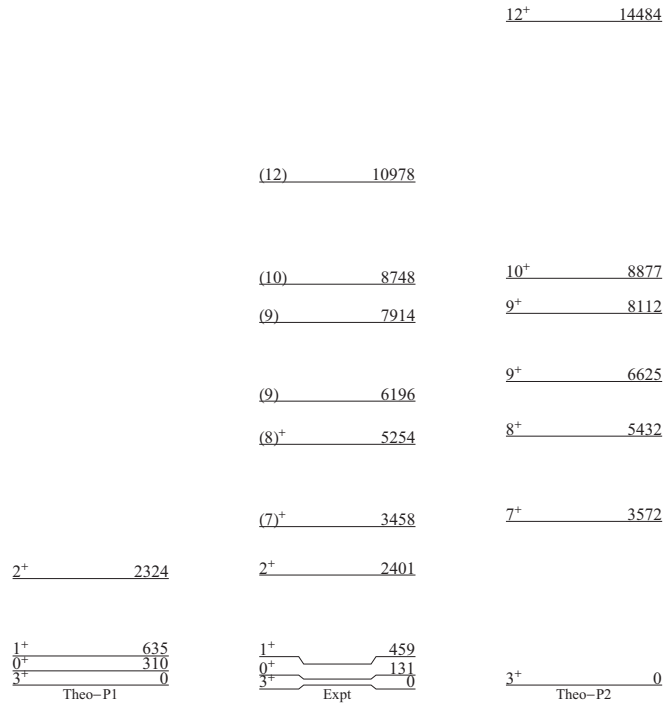

FIG. 8. Comparison of theoretical (Theo-P1 and Theo-P2) and experimental (Expt.) level energies of positive-parity states in ^{38}K. All these energies are plotted considering the ground-state energy (-251.345 MeV) as zero.

TABLE III. Comparison of experimental and theoretical reduced transition probabilities for different transitions in ^{38}K.

E_X	τ_{mean}(ps)		E_γ		$B(E3)$ (e^2 fm^6)			$B(M1)$ ($\times 10^{-3}\mu_N^2$)		$B(E2)$ (e^2 fm^4)	
keV	Reported [1]	J_i^π	keV	J_f^π	Expt.	Theor$_1$	Theor$_2$	Expt.	Theor.	Expt.	Theor.
459	10.1(9)	1^+	328	0^+				159(16)	295		
2401	0.075(22)	2^+	1942	1^+				103(31)	120		
2646	1414(144)	4^-	33	3^-				9(1)	7.6		
		4^-	2187	1^+	76(9)	30.4	68.3				
3420	101(14)	6^-	774	4^-						16.4 (24)	14.9
		6^-	3420	3^+	1346(198)	289	650				
3458	31.7(2) μs	7^+	812	4^-	44.6(22)	20	44.9				
6196	0.127[a]	9_1^+	2738	7^+							41.3
8692	3.15[a]	11^-	1296	9^-							67.5

[a]Estimated from calculated $B(E2)$ values.

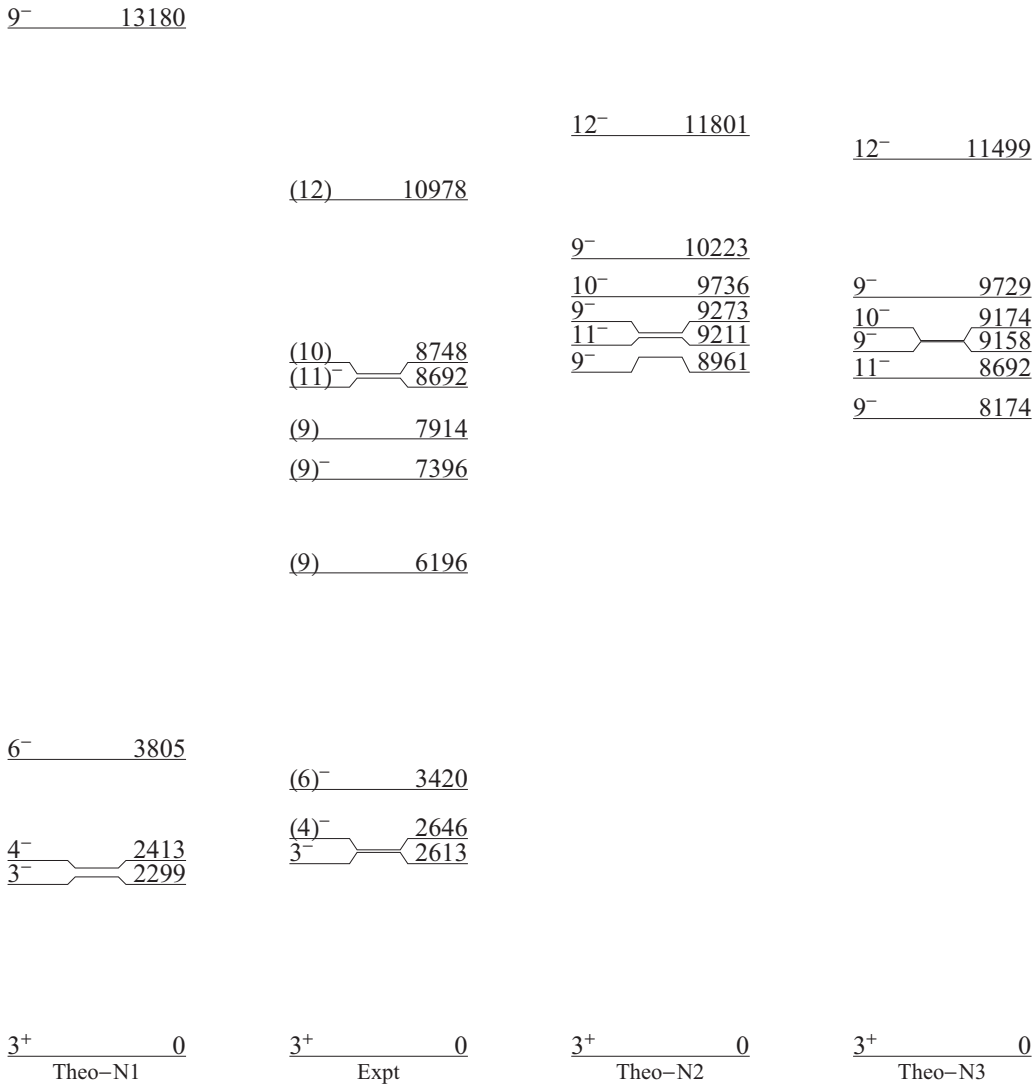

FIG. 9. Comparison of theoretical (Theo-N1, Theo-N2, and Theo-N3) and experimental (Expt.) level energies of negative-parity states in ^{38}K. All these energies are plotted with respect to the ground-state energy (−251.345 MeV) as zero.

calculated energy for the $J = 12$ level is overpredicted by several MeV, as shown in Fig. 8.

B. Negative-parity states

For the negative-parity states, three different truncation schemes (Theo-N1, Theo-N2, and Theo-N3) are adopted.

1. Theo-N1

In Theo-N1, we excite one nucleon into the pf shell (1p-1h excitation) to reproduce the negative-parity states. The mass-normalization factor for this calculation is 37. In this calculation, the first three negative-parity states [3^-, $(4)^-$, and $(6)^-$] were reproduced with a deviation up to 400 keV. However, the calculated energy of the 9^- state is overpredicted by several MeV. Since the maximum possible spin which can be generated in 1p-1h excitation is 10^-, we could not generate $J = 11$ and 12 states in this calculation.

2. Theo-N2 and Theo-N3

It is known that overpredicted energies may indicate the inadequacy of the model space. Results can be improved by increasing the contribution from pf orbitals by exciting more particles to the orbitals. Therefore, for the high-spin negative-parity states, we consider three-particle (3p-3h) excitations to the pf shell. We performed the 3p-3h excitation calculation with the full sd-pf model space (Theo-N2) but we could not calculate the transition matrix elements due to the dimensionality problem. To overcome the dimensionality problem, we therefore kept the $1d_{5/2}$ orbital full and reduced the single-particle energy (SPE) of each of the pf orbitals by an amount of 1.86 MeV to reproduce the experimental energy (8692 keV) of the 11^- level [Theo-N3]. Since the calculated energy of the 11^- level is well reproduced (energy deviation ≈500 keV) in Theo-N2 (Fig. 9), we have chosen the 11^- level for energy normalization. The mass normalization factor is 35 for both Theo-N2 and Theo-N3.

In Fig. 9, we compare the calculated energies of the negative-parity states (Theo-N3) with the experimental energies. It shows that, if we consider the newly observed 6196 and 7914 keV states ($J = 9$) as negative-parity levels, then all the 9^- states are overpredicted by several MeV (Fig. 9). Since their energies are close to the 9^+ levels (Theo-P2 of Fig. 8), we tentatively assign them as positive-parity levels. We therefore compare the calculated energy of the yrast 9^- state with the observed 7396 keV yrast 9^- state. It is found that the calculated energy of the yrast 9^- state in Theo-N3 is overpredicted by 778 keV. We have already mentioned that the 9^- level can be generated from 1p-1h excitations. The calculated energy of the 9^- level generated from 1p-1h excitation is 13 180 keV, as shown in Theo-N1. So this deviation may be due to the mixing of 1p-1h configuration into the 3p-3h configuration. Hence, a phenomenological approach following the discussion in Ref. [29], using two-level mixing between pure 3p-3h and 1p-1h states, was used to extract the extent of configuration mixing in 9^-. In this calculation, the 9^- state was assumed to be dominated by the 3p-3h configuration with a small amount of 1p-1h configuration mixing. Using the unperturbed energies of the yrast 9^- state obtained from pure 1p-1h and 3p-3h calculations, the experimental energy of the 9^- state was reproduced by considering the mixing coefficient of the 1p-1h configuration as a variable. The result shows that 11.8% of 1p-1h configuration mixing reproduces the experimental energy of the yrast 9^- state. It should be noted that the mixing of configurations from different np-nh ($n\hbar\omega$, $n = 0$, 1, 2, 3, 4, 6, 8) excitations on a particular positive- or negative-parity excited state have already been reported in the neighboring ^{36}Ar, ^{37}Ar, ^{38}Ar, and ^{40}Ca nuclei [7,11,30].

For the 8748 keV level ($J = 10$), the calculated energy of 10^- is 9174 keV (Theo-N3), which is 297 keV more than the calculated energy of the 10^+ level (Theo-P2). The calculated energy of the 10^+ level (8877 keV) is closer to the experimental energy of the $J = 10$ level than the calculated energy of the 10^- level (9174 keV). The parity of the 8748 keV ($J = 10$) level is therefore assigned tentatively as a positive-parity level.

In the case of the 10 978 keV ($J = 12$) level, we compare the experimental energy with the calculated energy of the 12^- level. In Theo-N3, the calculated energy of the 12^- level has been improved but still overpredicts by 521 keV. In Theo-P2, the calculated energy of the 12^+ level is overpredicted by more than 3 MeV. So, the 10 978 keV level ($J = 12$) is assigned tentatively as a negative-parity level.

C. Two-nucleon transfer spectroscopic factor calculation

In this section, we present our calculation of the two-nucleon transfer spectroscopic factors and their relevance to the J^π assignment of the levels in ^{38}K. In the present work, we assign the spins and parities of the 5254, 7396, 8692, 8748, and 10 978 keV levels as 8^+, 9^-, 11^-, $10^{(+)}$, and $12^{(-)}$, respectively. Previously these levels were assigned as $((9^+))$, $((10^-))$, $((12^-))$, $((11^-))$, and $((13^-))$, respectively [17]. They assigned the spins and parities of these levels by comparing the level scheme of ^{38}K above the isomer with the properties of low-lying ^{36}Ar states. They suggested that the high-spin states of ^{38}K have largely the structure of a

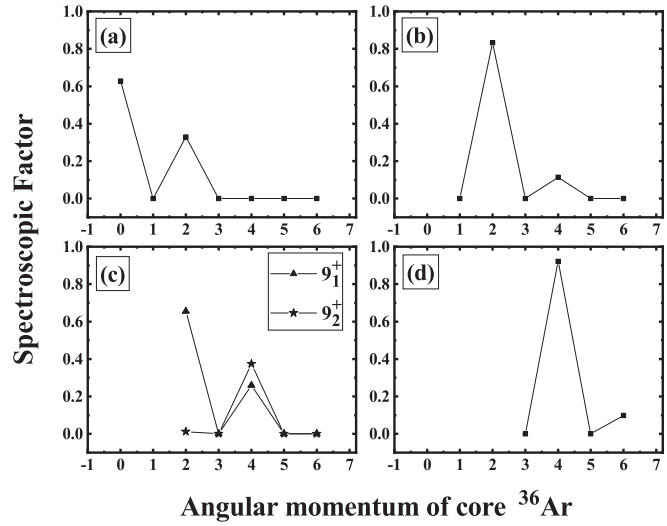

FIG. 10. Calculated spectroscopic factors for (a) 7^+, (b) 8^+, (c) 9^+, and (d) 10^+ states in ^{38}K to estimate the contribution of the low-lying positive-parity states of the core nucleus, ^{36}Ar.

$(f_{7/2})^2_{7,0}$ pair coupled to the appropriate states of ^{36}Ar, i.e., the $(7)^+$ and $((9^+))$ states were generated from 0^+ and 2^+ states, respectively, and the remaining negative-parity states, $((10^-))$, $((11^-))$, $((12^-))$, and $((13^-))$ states were generated from the core angular-momentum states 3^-, 4^-, 5^-, and 6^- of ^{36}Ar, respectively.

To verify this argument, two-nucleon transfer spectroscopic factor calculations have been carried out by using a LBSM calculation. We couple two nucleons (1 proton + 1 neutron) in the pf shell to the observed low-lying positive- and negative-parity states of ^{36}Ar to obtain the parentage of the high-spin positive- and negative-parity states of ^{38}K in terms of two-nucleon transfer spectroscopic factors. The low-lying positive- and negative-parity states of ^{36}Ar are generated from 0p-0h and 1p-1h excitation, respectively. In ^{38}K, the positive- and negative-parity states above the 3.458 MeV isomer have 2p-2h and 3p-3h configuration, respectively. In a two-nucleon transfer spectroscopic factor calculation, for a particular state of ^{38}K, the number of contributions from different pf orbitals for different ΔJ (depending on the core angular momentum and the angular momentum of the state of interest) increases considerably. Therefore, in our calculation, we consider only the contributions having spectroscopic amplitude $\geqslant$0.05. The calculated spectroscopic factors, i.e., the square of the spectroscopic amplitude, for the positive- and negative-parity states of ^{38}K, are shown in Figs. 10 and 11. It shows a strong correlation between the high-spin states of ^{38}K and the low-lying states of ^{36}Ar. It is found that the 7^+, 8^+, and $10^{(+)}$ states of ^{38}K are primarily generated from the low-lying 0^+, 2^+, and 4^+ states of ^{36}Ar, respectively. For the negative-parity states, the 9^-, 11^-, and $12^{(-)}$ states are generated from the core angular momentum 5^- and 6^- states, respectively. The 9_1^+ state has also a large spectroscopic factor (0.66) for the core angular-momentum state 2^+ but smaller than the 8^+ state (0.83). It has also been found that the calculated spectroscopic factor for the 10^+ level (0.92)

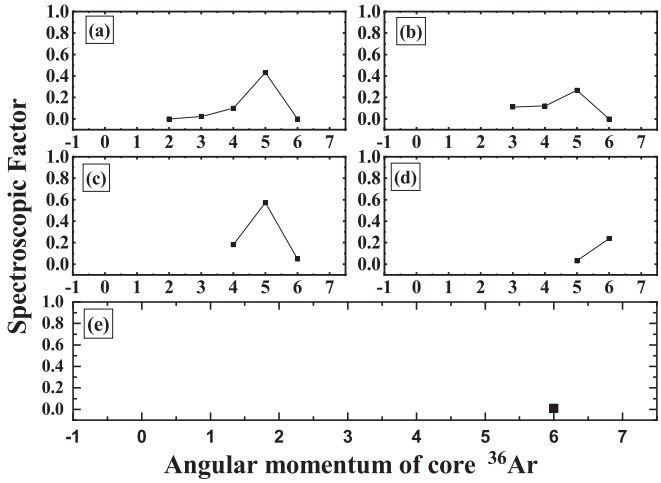

FIG. 11. Calculated spectroscopic factors for (a) 9^-, (b) 10^-, (c) 11^-, (d) 12^-, and (e) 13^- states in ^{38}K to estimate the contribution of the low-lying negative-parity states of the core nucleus, ^{36}Ar.

is higher than the 10^- level (0.27). The results obtained from two-nucleon transfer spectroscopic factor calculation, therefore, support our new spin-parity assignment of the levels above the isomer.

D. Configuration mixing and collectivity

The decomposition of the wave functions for the positive- and negative-parity states in ^{38}K are shown in Tables IV and V, respectively. For the low-lying positive- and negative-parity states below the isomer, we use the results obtained from 0p-0h and 1p-1h excitations, respectively. Similarly, for the high-spin positive- ($\geqslant 7^+$) and negative-parity ($\geqslant 9^-$) states, 2p-2h and 3p-3h excitations are considered. In the case of 3p-3h calculation, the $1d_{5/2}$ orbital was kept full to overcome the dimensionality problem.

A general particle partition is given by $(\Gamma_1^{m_1} \otimes \Gamma_2^{m_2} \otimes \cdots \otimes \Gamma_n^{m_n})$, where $m_1 + m_2 + \cdots + m_n = m$, with m being the total number of valence particles and $\Gamma \equiv (J, T)$ represents the spin-isospin of orbitals of the valance space. Due to various intermediate coupling of angular momenta and isospins, the particle partition has many different configurations. The probability and the structure (i.e., $m_1, m_2, \ldots, m_n$) of different partitions having $>10\%$ contribution are shown in Tables IV and V. The partitions are given in terms of occupation numbers of single-particle valence states. Here, N_1 is the total number of particle partitions for a particular state, each with contribution $>1\%$, and N_2 gives an estimate of the minimum number of particle partitions, each of which contributes $\leqslant 1\%$ in the state.

Table IV shows that the low-lying positive-parity states (3^+, 0^+, 1^+, and 2^+) are primarily generated from single-particle excitations. They have a much smaller extent of configuration mixing with the largest contribution $\approx 97\%$ from the single partition. However, the configuration mixing in terms of single-particle partitions for the high-spin positive-parity states (7^+–10^+) has been increased. It has been found that they have 9–12 particle partitions that contribute at least 1% with the largest 25%–45% in their wave function. These high-spin positive-parity states, therefore, show substantial configuration mixing in terms of particle partitions, which give us a sign of the presence of collective excitations at higher excitation energy in ^{38}K. For the negative-parity states (Table V), a relatively smaller extent of configuration mixing is observed. States with 1p-1h configuration have 5 to 6 particle partitions with the largest 86% and states with 3p-3h

TABLE IV. Structure of the wave functions for the positive-parity states in ^{38}K. The partitions are given in terms of occupation numbers of single-particle valence states in the following order: $1d_{5/2}$, $1d_{3/2}$, $2s_{1/2}$, $1f_{7/2}$, $1f_{5/2}$, $2p_{3/2}$, and $2p_{1/2}$.

		Energy (MeV)		Wave function			
J_i^π	T	Expt.	Theor.	%	Partition	N_1	N_2
3_1^+	0	−251.165	0(−251.345)	97	[12,6,4,0,0,0,0]	2	1
0_1^+	1	0.131	0.310	94	[12,6,4,0,0,0,0]	3	1
1_1^+	0	0.459	0.635	55	[12,7,3,0,0,0,0]	4	1
				20	[12,6,4,0,0,0,0]		
				16	[11,7,4,0,0,0,0]		
2_1^+	1	2.401	2.324	93	[12,6,4,0,0,0,0]	2	3
7_1^+	0	3.458	3.572	45	[12,4,4,2,0,0,0]	11	5
				13	[10,6,4,2,0,0,0]		
				11	[12,6,2,2,0,0,0]		
8_1^+	0	5.254	5.432	25	[12,5,3,2,0,0,0]	10	6
				23	[12,4,4,2,0,0,0]		
				13	[11,6,3,2,0,0,0]		
9_1^+	0	6.196	6.625	38	[12,4,4,2,0,0,0]	11	5
				13	[11,5,4,2,0,0,0]		
				12	[12,5,3,2,0,0,0]		
9_2^+	0	7.914	8.112	31	[12,4,4,2,0,0,0]	12	5
				18	[11,5,4,2,0,0,0]		
				15	[12,5,3,2,0,0,0]		
10_1^+	0	8.748	8.877	33	[11,5,4,2,0,0,0]	9	5
				15	[12,5,3,2,0,0,0]		
				11	[12,4,4,2,0,0,0]		

TABLE V. Structure of the wave functions for the negative-parity states in ^{38}K. The partitions are given in terms of occupation numbers of single-particle valence states in the following order: $1d_{5/2}$, $1d_{3/2}$, $2s_{1/2}$, $1f_{7/2}$, $1f_{5/2}$, $2p_{3/2}$, and $2p_{1/2}$.

		Energy(MeV)		Wave function			
J_i^π	T	Expt.	Theor.	%	Partition	N_1	N_2
3_1^-	0	2.613	2.299	80	[12,5,4,1,0,0,0]	6	4
4_1^-	0	2.646	2.413	82	[12,5,4,1,0,0,0]	6	3
6_1^-	0	3.420	3.805	86	[12,5,4,1,0,0,0]	5	3
9_1^-	0	7.369	8.174	48	[12,3,4,3,0,0,0]	9	5
				28	[12,3,4,2,0,1,0]		
11_1^-	0	8.692	8.692	71	[12,3,4,3,0,0,0]	7	2
				12	[12,4,3,3,0,0,0]		
12_1^-	0	10.978	11.499	53	[12,3,4,3,0,0,0]	7	2
				34	[12,4,3,3,0,0,0]		

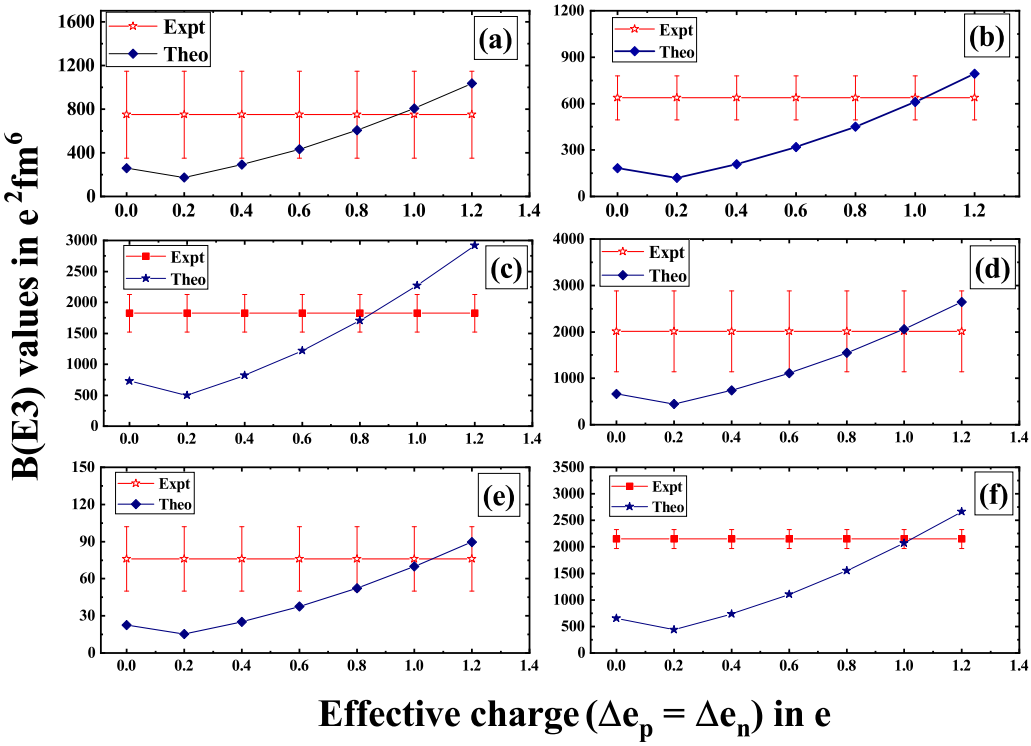

FIG. 12. Experimental and theoretical $B(E3)$ values for a few transitions, viz., (a) 4232 keV of ^{30}P, (b) 4431 keV of ^{31}P, (c) 5006 keV of ^{32}S, (d) 4597 keV of ^{34}Cl, (e) 2418 keV of ^{38}Ar, and (f) 3597 keV of ^{39}K, as a function of effective charge.

configuration have 7 to 9 particle partitions with the largest 71% in their wave functions.

The reduced transition probabilities $B(M1)$, $B(E2)$, and $B(E3)$ for a few transitions below the isomer have been calculated by using the effective charges $e_p = 1.5e$ and $e_n = 0.5e$ and free values of g factors. The calculated value of $M1$ and $E2$ strengths show good agreement with the corresponding experimental data (Table III), which provide evidence in favor of the reliability of the calculated wave functions. However, the calculated $B(E3)$ strengths are suppressed by a factor of two or more (Theor$_1$). We also calculated the $E3$ strengths for a few other sd-shell nuclei using the effective charges $e_p = 1.5e$ and $e_n = 0.5e$. For all cases, the calculated strengths are suppressed. So, we have to optimize the proton and neutron effective charges for $E3$ transitions. In Fig. 12, the calculated $B(E3)$ values are compared with the experimental $B(E3)$ values for a few sd-shell nuclei. The experimental transition strengths are calculated from the reported branching, mixing ratios, and level lifetimes [1]. We calculated the $B(E3)$ strengths of these nuclei for different effective charges ($\Delta e_p = \Delta e_n$). The different particle restrictions mentioned in Refs. [3,31–33] are used to reproduce the wave functions of the levels of interest in ^{30}P, ^{31}P, ^{32}S, ^{34}Cl, ^{38}Ar, and ^{39}K. It clearly shows that, in most of the cases, the calculated $B(E3)$ values agree well with the experimental values for $e_p = 2.0e$ and $e_n = 1.0e$. In ^{38}K, we have therefore calculated the $B(E3)$ strengths by using the effective charges $e_p = 2.0e$ and $e_n = 1.0e$ (Theor$_2$). We have an excellent improvement in the calculated $B(E3)$ value, as shown in Table III.

The transition strengths for a few $E2$ transitions above the isomer have also been calculated by using the effective charges $e_p = 1.5e$ and $e_n = 0.5e$. We estimated the mean lifetime (τ_m) of the 6196 and 8692 keV levels from the calculated $B(E2)$ strengths of the 2738 and 1296-keV transitions. The branching of the 1296 keV transition was estimated from the measured relative intensities of the 778 and 1296 keV transitions. The results are also shown in Table III. All calculations have been carried out for $\Delta T = 0$ transition only.

E. Prediction of deformed band in ^{38}K

Collectivity, large deformation, and even superdeformation at higher excitation energies, has been observed in a few upper sd-shell nuclei [2–4]. Not only the neighboring nuclei, collective excitations, and deformed band structures have also been observed in the isobaric nucleus ^{38}Ar, and shell-model calculations suggest a 4p-4h configuration of these bands [16]. In the present work, we investigate the structure of ^{38}K up to 11 MeV excitation energy and theoretically interpret them by using 0p-0h, 1p-1h, 2p-2h, and 3p-3h excitations in shell-model calculations. Collective excitations in terms of large configuration mixing have been found in the high-spin positive-parity states. However, no band-like structure has been observed at higher excitation energies. The calculated $E2$ strengths of the observed $E2$ transitions are also small. So, we have extended our theoretical investigation by using 4p-4h excitations to search for collectivity in ^{38}K. As the full-space calculation was not possible, the $1d_{5/2}$ orbital was kept completely filled up for this calculation and reduced the single-particle energy (SPE) of each of the pf orbitals by 1.86 MeV.

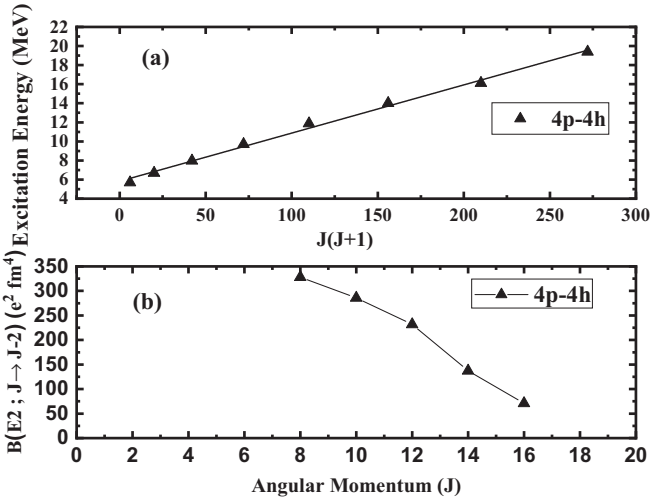

FIG. 13. (a) Calculated excitation energies and (b) $B(E2)$ values for the positive-parity states generated from 4p-4h excitation in ^{38}K.

In Fig. 13(a), we plot the excitation energies of the levels with $J(J+1)$. The plot shows a very good linear variation of the level energies with $J(J+1)$. The details of the wave functions of the levels generated from the 4p-4h calculation are shown in Table VI. The table shows large configuration mixings in terms of particle partitions for all the levels. Probability and the structure (i.e., $m_1, m_2, \ldots, m_n$) of different partitions having >10% contribution for 4p-4h excitation are given in Table VI.

TABLE VI. Structure of the wave functions for the positive-parity states in ^{38}K generated from 4p-4h truncation. The partitions are given in terms of occupation numbers of single-particle valence states in the following order: $1d_{5/2}$, $1d_{3/2}$, $2s_{1/2}$, $1f_{7/2}$, $1f_{5/2}$, $2p_{3/2}$, and $2p_{1/2}$.

		Energy (MeV)	Wave function			
J_i^π	T	Theor.	%	Partition	N_1	N_2
2_1^+	0	5.686	11	[12,4,2,4,0,0,0]	22	20
			16	[12,3,3,4,0,0,0]		
4_1^+	0	6.696	13	[12,3,3,4,0,0,0]	25	17
6_1^+	0	7.978	11	[12,3,3,3,0,1,0]	21	18
			12	[12,3,3,4,0,0,0]		
8_1^+	0	9.703	11	[12,3,3,3,0,1,0]	20	15
			14	[12,3,3,4,0,0,0]		
10_1^+	0	11.879	11	[12,3,3,3,0,1,0]	18	11
			18	[12,3,3,4,0,0,0]		
12_1^+	0	13.999	11	[12,4,2,4,0,0,0]	11	8
			14	[12,3,3,3,0,1,0]		
			21	[12,3,3,3,0,0,1]		
			14	[12,2,4,4,0,0,0]		
14_1^+	0	16.111	16	[12,3,3,4,0,0,0]	7	6
			15	[12,3,3,3,0,1,0]		
			20	[12,2,4,4,0,0,0]		
			19	[12,2,4,3,0,1,0]		
16_1^+	0	19.390	14	[12,3,3,3,1,0,0]	5	1
			70	[12,3,3,4,0,0,0]		

We also calculated the $B(E2)$ values to extract the deformation. Although we calculated the energies of all the levels generated from 4p-4h excitations, we could not calculate the $B(E2)$ values for the $6^+ \rightarrow 4^+$ and $4^+ \rightarrow 2^+$ transitions due to computational limitations. The results are shown in Fig. 13(b). It shows large $B(E2)$ values for the positive-parity band generated from 4p-4h excitation. The deformation parameter β for the $B(E2)$ values 328 e^2 fm^4 ($8^+ \rightarrow 6^+$) is ≈0.38 [34]. Estimated major-to-minor axis ratio (X) [34] is 1.42 for $\beta = 0.38$. These values are comparable to the observed deformation in ^{40}Ca [8], ^{36}Ar [9], and ^{35}Cl [10]. Therefore, our calculations provide a strong indication of the presence of a deformed band at higher excitation energies in ^{38}K.

V. CONCLUSION

High-spin states of ^{38}K above the 31.67 μs isomer populated through the ^{12}C(^{28}Si, np)^{38}K reaction with a 110 MeV ^{28}Si beam have been studied by using the Indian National Gamma Array facility. Two new levels and four new transitions have been added to the existing level scheme. The spins and parities of most of the levels have been assigned, modified, or confirmed from $R_{\rm DCO}$ and linear polarization measurements. For a few weak transitions, $R_{\rm ADO}$ measurements have been carried out to assign their dipole or quadrupole nature. The multipole mixing ratios (δ) for a few transitions have been measured. Large-basis shell-model calculations were performed to understand the microscopic origin of these levels. In our calculations, different particle restrictions in sd- and pf-shell orbitals were used to reproduce the experimental level scheme. For the levels above the isomer, two-nucleon transfer spectroscopic factors were calculated to establish that the excited (positive- and negative-parity) levels in ^{38}K have ^{36}Ar (core) plus two-nucleon structure. The experimental transition strengths for a few transitions below the isomer were compared with the calculated values. Collective excitations at higher excitation energy were studied. We also predicted the presence of a deformed band generated with the 4p-4h configuration in ^{38}K.

ACKNOWLEDGMENTS

The authors acknowledge the help from all other INGA collaborators and the Pelletron staff of IUAC for their support and cooperation. Special thanks are due to Pradipta Das for his technical help for target preparation and to the Pelletron staff for a nearly uninterrupted beam. One of the authors (R.R.) would like to express her deep gratitude towards SERB-DST, Government of India (Project No. EMR/2016/006339), for the generous financial support. This work was also partially funded by the research grant (Project No. EMR/2016/006339) from SERB-DST, Government of India. The Department of Science and Technology (Grant No. IR/S2/PF-03/2003-III), Government of India, is thankfully acknowledged for the Indian Gamma Array Collaboration.

[1] http://www.nndc.bnl.gov.
[2] A. Bisoi *et al.*, Phys. Rev. C **90**, 024328 (2014).
[3] A. Bisoi *et al.*, Phys. Rev. C **89**, 024303 (2014).
[4] F. Della Vedova *et al.*, Phys. Rev. C **75**, 034317 (2007).
[5] R. Kshetri *et al.*, Nucl. Phys. A **781**, 277 (2007).
[6] S. Aydin *et al.*, Phys. Rev. C **86**, 024320 (2012); **89**, 014310 (2014).
[7] A. Das *et al.*, Phys. Rev. C **101**, 044310 (2020).
[8] E. Ideguchi *et al.*, Phys. Rev. Lett. **87**, 222501 (2001); C. J. Chiara, E. Ideguchi, M. Devlin, D. R. LaFosse, F. Lerma, W. Reviol, S. K. Ryu, D. G. Sarantites, C. Baktash *et al.*, Phys. Rev. C **67**, 041303(R) (2003).
[9] C. E. Svensson *et al.*, Phys. Rev. Lett. **85**, 2693 (2000); Phys. Rev. C **63**, 061301(R) (2001).
[10] A. Bisoi *et al.*, Phys. Rev. C **88**, 034303 (2013).
[11] E. Caurier, J. Menèndez, F. Nowacki, and A. Poves, Phys. Rev. C **75**, 054317 (2007).
[12] E. Caurier, F. Nowacki, and A. Poves, Phys. Rev. Lett. **95**, 042502 (2005).
[13] T. Sakuda and S. Ohkubo, Phys. Rev. C **49**, 149 (1994).
[14] T. Sakuda and S. Ohkubo, Nucl. Phys. A **744**, 77 (2004); **748**, 699 (2005).
[15] A. Bisoi *et al.*, Phys. Rev. C **97**, 044317 (2018).
[16] D. Rudolph *et al.*, Phys. Rev. C **65**, 034305 (2002).
[17] C. J. van der Poel *et al.*, Nucl. Phys. A **394**, 501 (1983).
[18] A. Bisoi *et al.*, Proc. DAE-BRNS Symp. Nucl. Phys. (India) **61**, 106 (2016); http://www.sympnp.org/proceedings.
[19] S. Muralithar *et al.*, Nucl. Instrum. Methods Phys. Res., Sect. A **622**, 281 (2010); S. Ray *et al.*, Proc. DAE-BRNS International Symp. Nucl. Phys. (India) **54**, 56 (2009).
[20] R. Bhowmick *et al.*, Proc. DAE-BRNS Symp. Nucl. Phys. (INDIA)B **44**, 422 (2001); https://www.sympnp.org/proceedings.
[21] M. Saha Sarkar *et al.*, Nucl. Instrum. Methods Phys. Res., Sect. A **491**, 113 (2002).
[22] A. Gavron, Phys. Rev. C **21**, 230 (1980).
[23] E. S. Macias, W. D. Ruhter, D. C. Camp, and R. G. Lanier, Comput. Phys. Commun. **11**, 75 (1976).
[24] M. Piiparinen, A. Ata¸c, J. Blomqvist, G. B. Hagemann, B. Herskind, R. Julin, S. Juutinen, A. Lampinen, J. Nyberg, G. Sletten *et al.*, Nucl. Phys. A **605**, 191 (1996).
[25] K. Starosta *et al.*, Nucl. Instrum. Methods Phys. Res., Sect. A **423**, 16 (1999).
[26] B. A. Brown, A. Etchegoyen, W. D. M. Rae, and N. S. Godwin, MSU-NSCL Report No. 524 (1985).
[27] E. K. Warburton, J. A. Becker, and B. A. Brown, Phys. Rev. C **41**, 1147 (1990).
[28] G. Audi, A. H. Wapstra, and C. Thibault, Nucl. Phys. A **729**, 337 (2003); B. J. Cole, J. Phys. G: Nucl. Phys. **11**, 351 (1985).
[29] P. J. Brussard and P. W. M. Glaudemans, *Shell-Model Applications in Nuclear Spectroscopy* (North-Holland, Amsterdam, 1977); R. F. Casten, *Nuclear Structure from a Simple Perspective* (Oxford University Press, New York, 1990).
[30] S. Courtin *et al.*, J. Phys.: Conf. Ser. **436**, 012051 (2013); A. F. Lisetskiy *et al.*, Nucl. Phys. A **789**, 114 (2007).
[31] I. Ray *et al.*, Phys. Rev. C **76**, 034315 (2007).
[32] A. Kangasmäki, P. Tikkanen, J. Keinonen, W. E. Ormand, S. Raman, Zs. Fülöp, Á. Z. Kiss, and E. Somorjai, Phys. Rev. C **58**, 699 (1998).
[33] Th. Andersson *et al.*, Eur. Phys. J. A **6**, 5 (1999).
[34] http://www.physics.mcmaster.ca/~balraj/sdbook/.